



Loading Direction Dependence of Yield-Point Phenomenon and Bauschinger Effect in API X70 Steel Sheet

Hyung Lae Kim¹ · Sung Hyuk Park²

Received: 18 April 2019 / Accepted: 7 June 2019 / Published online: 28 June 2019
© The Korean Institute of Metals and Materials 2019

Abstract

In this study, variations in the tensile behavior and Bauschinger effect with the applied loading direction in an American Petroleum Institute (API) X70 steel sheet are investigated by conducting tensile and strain-reversal tests along the rolling direction (RD), the transverse direction (TD), and a direction inclined at an angle of 45° from the RD to the TD (45D). The microstructure of the rolled steel sheet consists of polygonal ferrite and acicular ferrite, and it has a rolling texture that is typical of body-centered cubic metal materials. During tensile deformation, the yield-point phenomenon, which involves occurrence of discontinuous yielding and development of Lüders strain, occurs in all the loading directions. However, the material shows a lower yield strength and larger Lüders strain under tension along the 45D than under tension along the RD and TD. The Bauschinger effect, which occurs under subsequent reversal tension after compression, is also more pronounced under loading along the 45D. These results are attributed to the fact that dislocation slips are activated more easily under deformation along the 45D, which is evidenced by the lower Taylor factor and larger number of active slip systems under loading along the 45D. Furthermore, results of viscoplastic self-consistent simulation reveal that along all the directions, the $\{112\} <111>$ slip system is vigorously activated during tensile and compressive deformations and that its activation plays an important role in the deformation behavior and yield strength of the material.

Keywords Line-pipe steel · Mechanical properties · Bauschinger effect · Texture · Dislocation slip

1 Introduction

In the last few decades, line-pipe steels have been extensively developed—from American Petroleum Institute (API) 5L X52 grade to API X120 grade—in order to cope with demands for their use at various operating pressures and in diverse operating environments, as well as to meet the requirement of lower transmission costs. Line pipes are generally fabricated from hot-rolled steel coils via pipe manufacturing processes consisting of leveling, pipe forming, and welding. Unlike seamless-pipe manufacturing processes, these welded-pipe manufacturing processes can provide large pipes without any limitations in size, and welded

pipes are cheaper than the corresponding seamless pipes. Welded line pipes are typically manufactured by either electric resistance welding (ERW) or spiral submerged arc welding (SAW). In the ERW process, a leveled steel strip is bent along the longitudinal direction and its two edges are welded together without the use of a filler material, which consequently gives a continuous pipe (Fig. 1a). In the SAW process, a leveled steel strip is formed in a spiral loop by the use of a spiral forming machine and a solid filler material, after which this spiral loop is welded from the inside and outside of the pipe (Fig. 1b). Line pipes produced by these processes are classified into grades according to specifications established by the API, which are based on the yield strength along the circumferential direction of line pipes. When hot-rolled steels have a specific rolling texture, their yield strength can change significantly with the applied loading direction owing to differences in the number and activity of activated slip systems in different loading directions. In the case of a pipe manufactured by SAW, its yield strength along the circumferential direction is almost the same as the yield strength along the rolling direction (RD) of the initial

✉ Sung Hyuk Park
sh.park@knu.ac.kr

¹ SMR Fuel Development Team, Korea Atomic Energy Research Institute (KAERI), Daejeon 34057, Republic of Korea

² School of Materials Science and Engineering, Kyungpook National University, Daegu 41566, Republic of Korea

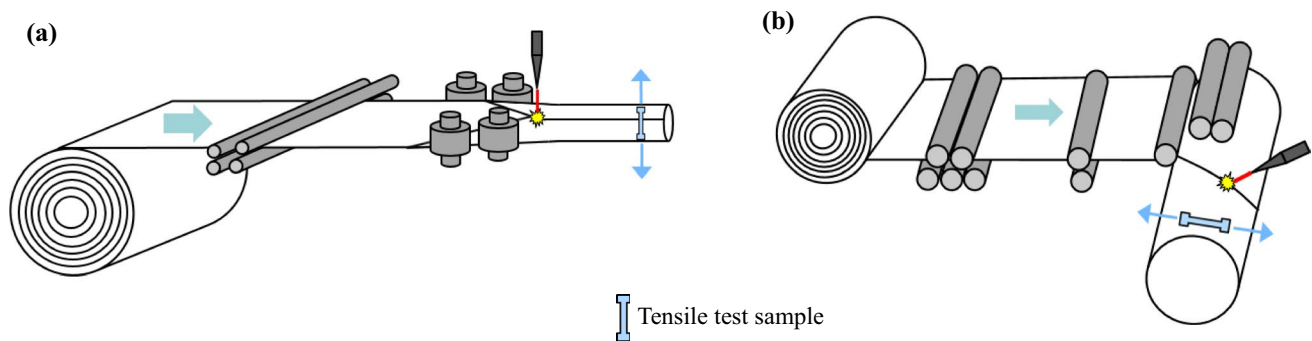


Fig. 1 Schematic diagrams of pipe manufacturing processes: **a** electric resistance welding (ERW) and **b** spiral submerged arc welding (SAW)

hot-rolled coil, as shown in Fig. 1b. In contrast, the yield strength of a pipe manufactured by ERW corresponds to the yield strength along the transverse direction (TD) of the initial hot-rolled coil, as shown in Fig. 1a. Since the yield strengths along the RD and TD of an initial hot-rolled steel sheet can differ according to the rolling texture, the yield strength along the circumferential direction of the fabricated pipe can also vary with the pipe manufacturing process (e.g., ERW and SAW) [1–3]. This means that even when the same rolled steel sheet is used for the fabrication of pipes, the final API grade of the pipes can differ according to the employed manufacturing process.

In addition, the yield strength of hot-rolled steel coils can decrease owing to compressive or tensile strain imposed during the leveling, piping, and flattening processes. When a material is compressed or tensioned along a certain direction and then subsequently deformed along the reverse direction, the yield strength of the deformed material is lower than that of the corresponding undeformed material [4–6]; this phenomenon is termed the Bauschinger effect. The Bauschinger effect strengthens proportionally with an increase in the number of mobile dislocations formed by previously imposed plastic deformation. The movement of mobile dislocations is strongly affected by microstructural characteristics such as crystal structure, grain size, texture, and presence of precipitates. Several studies have shown that the yield strength of rolled steel coils varies considerably with the amount of precipitates and the forming strain t/D (where t and D are the thickness of the rolled coil and the pipe diameter, respectively) [7–12]. Choi et al. [13] also reported that the Bauschinger effect weakened with an increase in the amount of acicular ferrite (AF), which resulted in the continuous yielding phenomenon. In another study, the change in the yield strength with the amount of previous deformation was investigated on the basis of the correlation between the strain hardening behavior and the Bauschinger effect [14]. There is additionally a need for systematic investigation of the variation in the yield strength of steel sheets with the loading direction in order to understand the relationship

among the initial rolling texture, slip deformation behavior, and resultant mechanical properties of rolled steel sheets. However, despite the fact the tensile loading direction, which governs the API grade of steel pipes, changes with the pipe forming method, few studies have investigated the loading direction dependence of yield strength and the influence of the initial rolling texture on the Bauschinger effect.

Therefore, in the present study, the influence of initial texture on the mechanical properties of rolled steel sheets was investigated using specimens obtained from a leveled line-pipe steel sheet along three different directions: the RD, the TD, and a direction inclined at an angle of 45° from the RD to the TD (hereafter referred to as “45D”). The yield strength and Bauschinger effect of the specimens were measured by tensile tests and strain-reversal tests, respectively. The slip behaviors during deformation in the three loading directions were compared via Taylor factor analysis performed using data obtained from electron backscatter diffraction (EBSD) measurements. In addition, the activity of each slip mode was identified by viscoplastic self-consistent (VPSC) simulation of deformation, and the texture evolution during tensile deformation was also analyzed by VPSC simulations. From these analyses, the loading direction dependence of the yield-point phenomenon and the relationship between the initial texture and the Bauschinger effect in a hot-rolled API steel sheet were established.

2 Experimental Procedure

An API X70 grade line-pipe steel sheet [chemical composition: 0.06C-1.6Mn (wt%)] with a minimum yield strength of 70 ksi (482 MPa) was used in this study. The steel sheet, having a fine grain structure, was fabricated by a thermo-mechanical control process: a hot slab was first rolled with a high rolling reduction of 80% at a temperature of 950°C in the non-recrystallized austenite region, after which it was subjected to finishing rolling at a relatively low temperature of 830°C in the austenite region in order to generate

numerous nucleation sites for ferrite formation; this was finally followed by rapid cooling to coiling temperatures of 580–600 °C with a cooling rate of 25 °C/s. After the sheet was polished with emery papers and etched in a 2% nital solution, its microstructure was observed by optical microscopy (OM). For EBSD measurements, the sample surface was progressively ground with emery papers and diamond pastes and then subjected to a final polish with colloidal silica to obtain a defect-free surface. EBSD data with a confidence index larger than 0.1 were analyzed using the TexSEM Laboratories Orientation Imaging Microscopy (TSL OIM) analysis software to examine the active slip systems.

For tensile and strain-reversal tests, round specimens with a gage diameter of 6.35 mm and gage length of 16 mm were machined from the sheet along the RD, TD, and 45D; these three specimens are hereafter referred to as RD, TD, and 45D samples, respectively. The tensile and strain-reversal tests were conducted at room temperature at a strain rate of 10^{-2} s^{-1} by means of a universal testing machine (Instron 8862). In the strain-reversal tests, a compressive strain of 2% was first applied to the samples because the compressive strain accumulated during a pipe manufacturing process is generally 2%–3% [15, 16]; then, the compressed samples were tensioned along the previous loading direction in order to estimate the Bauschinger effect. The 0.2%-offset flow stress and stress of the lower yield point were considered as the yield strengths of the samples showing continuous and discontinuous yielding behaviors, respectively. The tensile and strain-reversal tests for each loading condition were repeated two or three times to confirm the consistency of the results; for the sake of simplicity, a representative curve was used for each condition. Additionally, the slip modes activated during plastic deformation were identified via simulations using the VPSC model proposed by Tomé and Lebensohn [17, 18]. The developed textures determined from the EBSD analysis of the 20% tensioned samples were compared with those established by the VPSC simulations.

3 Results

Figure 2 shows the microstructures and textures of the API X70 steel sheet, which were obtained by OM observations and EBSD measurements. The microstructure consists of polygonal ferrite (PF) and AF, and the average grain size of the sheet is 10 μm (Figs. 2a, b). In addition, the sheet has a rolling texture typical of steels with a body-centered cubic (BCC) crystal structure [19]; the $\{001\} \langle 110 \rangle$, $\{112\} \langle 110 \rangle$, and $\{113\} \langle 110 \rangle$ preferred orientations develop along the α -fiber in the (001) and (100) pole figures, and the $\{111\} \langle 110 \rangle$ and $\{111\} \langle 112 \rangle$ preferred orientations develop along the γ -fiber in the (111) pole figure (Fig. 2c). The tensile stress–strain curves of the TD, 45D, and RD samples are shown in Fig. 3. These curves reveal that the yield strength of the sheet decreases in the following order of loading directions: TD (605 MPa) > RD (596 MPa) > 45D (587 MPa) (Table 1). The reasons for this

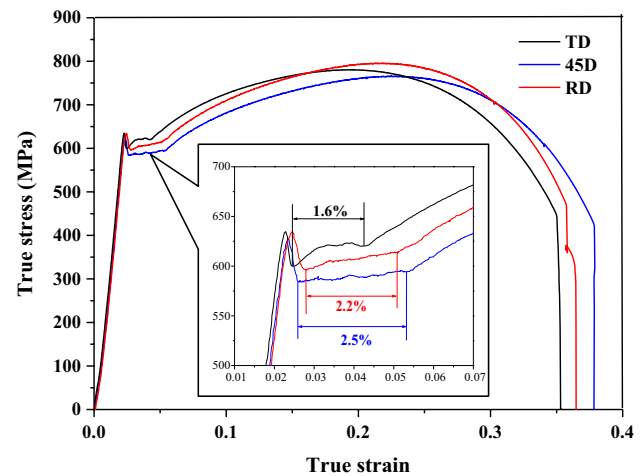


Fig. 3 Tensile stress–strain curves of API X70 steel sheet

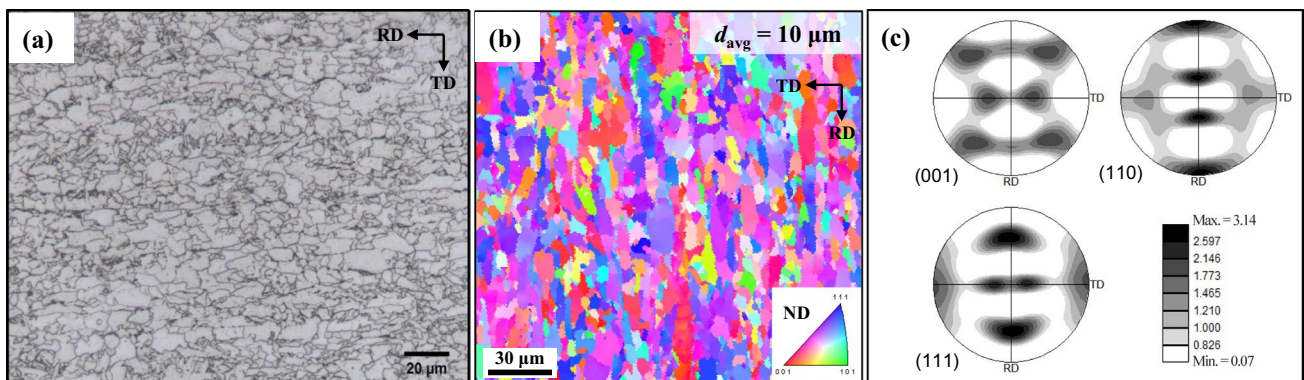


Fig. 2 a Optical micrograph and b, c EBSD measurement results of API X70 steel sheet: b inverse pole figure and c (001), (110), and (111) pole figures. d_{avg} denotes the average grain size

Table 1 Mechanical properties of API X70 steel sheet determined from tensile and strain-reversal tests in different loading directions

Test type	TD			45D			RD		
	YS (MPa)	TS (MPa)	EL (%)	YS (MPa)	TS (MPa)	EL (%)	YS (MPa)	TS (MPa)	EL (%)
Tensile test	605	779	35	587	764	38	596	795	36
Strain-reversal test	580	766	37	523	756	39	545	761	36

variation in the yield strength with the loading direction are discussed in Sect. 4, along with analyses of the Taylor factor and active slip systems under each loading condition.

The TD, 45D, and RD samples all clearly exhibit the yield-point phenomenon during tensile deformation (Fig. 3), which is easily observed in low-carbon steels with a BCC structure [20]. In a material consisting of phases with a low dislocation density (e.g., ferrite and pearlite), the yield-point phenomenon is related to the pinning of dislocations formed at the early stage of deformation to the interstitial solute atoms (e.g., carbon and nitrogen) and to the breakaway of the dislocations from their solute atmospheres [20, 21]. Since the microstructure of the steel sheet used in the present study consists of PF and AF—both of which have a relatively low dislocation density—the steel sheet exhibits an obvious yield-point phenomenon regardless of the applied loading direction. In addition, the yield-point phenomenon causes the formation of Lüders bands, which are locally deformed regions formed in the tensile specimen, because the dislocations formed during initial deformation become immobilized owing to pinning by interstitial atoms [21–24]. The Lüders bands propagate over a tensile specimen during yield elongation until they cover the entire surface of the specimen. As shown in Fig. 3, in this study, the yield elongation (i.e., Lüders strain) of the sheet varies with the applied loading direction; the yield elongation of the 45D sample is highest (2.5%), followed by the RD sample (2.2%) and the TD sample (1.6%). This order of the yield elongation (45D > RD > TD) is opposite to that of the yield strength (TD > RD > 45D). The variation in the yield elongation with the loading direction is related to the active slip modes and their activity under each deformation condition; this topic is discussed further in Sect. 4.

Figure 4 shows the tensile stress–strain curves of the 2% precompressed samples, which were obtained from the strain-reversal tests along the TD, 45D, and RD; for comparison, the corresponding tensile stress–strain curves of the initially undeformed samples are also included in this figure. The mechanical properties of the API X70 steel sheet as determined from the tensile and strain-reversal tests are listed in Table 1. It is noticeable that unlike in the tensile tests, in the strain-reversal tests, all the samples exhibit continuous yielding behavior, which is attributed to the formation of dislocations that are free from interstitial atoms owing to precompression. This indicates that in all the

directional samples, a considerable amount of mobile dislocations is formed under 2% compressive strain. Moreover, for all the samples, the yield strengths in the strain-reversal tests are lower than those in the tensile tests. This lower yield strength under the strain-reversal condition than under the tensile condition is well known as the Bauschinger effect, as described above. In polycrystalline metal materials, the Bauschinger behavior is associated with the reduction in the stress required for the occurrence of yielding during deformation when the direction of the applied strain is reversed [4–6, 25]. During the initial plastic deformation, numerous dislocations are formed and piled up at crystal barriers, i.e., grain boundaries. These pile-up dislocations can easily move along previously activated glide planes when the subsequent plastic deformation is applied along the reverse direction; this facilitates the yielding behavior and consequently leads to a decrease in the yield strength of the material. As shown in Fig. 4, the difference in the yield strength between the tensile test and the strain-reversal test is dependent on the loading direction. The decrease in the yield strength of the TD sample by the Bauschinger effect is relatively small, 25 MPa, whereas those of the 45D and RD samples are considerably large, 64 MPa and 51 MPa, respectively (Fig. 4 and Table 1). These results of the tensile and strain-reversal tests under deformation along the RD, TD, and 45D demonstrate that the yield strength and yield elongation of and the Bauschinger effect in the rolled steel sheet with an intense texture vary significantly with the applied loading direction.

4 Discussion

4.1 Taylor Factor Analysis under RD, 45D, and TD Loading Conditions

In materials with a specific texture, the variation in the extent of the Bauschinger effect with the loading direction can be explained using the relationship between the initial texture and the slip behavior in each deformation mode [26, 27]. Slip systems in BCC metals are more complicated than those in face-centered cubic (FCC) metals; in the latter, dislocation slip occurs along the close-packed <110> direction on the close-packed {111} plane [28]. In BCC metals, however, slip occurs along the <111> direction, which is a close-packed direction, and the {110}, {112}, and {123} slip planes can

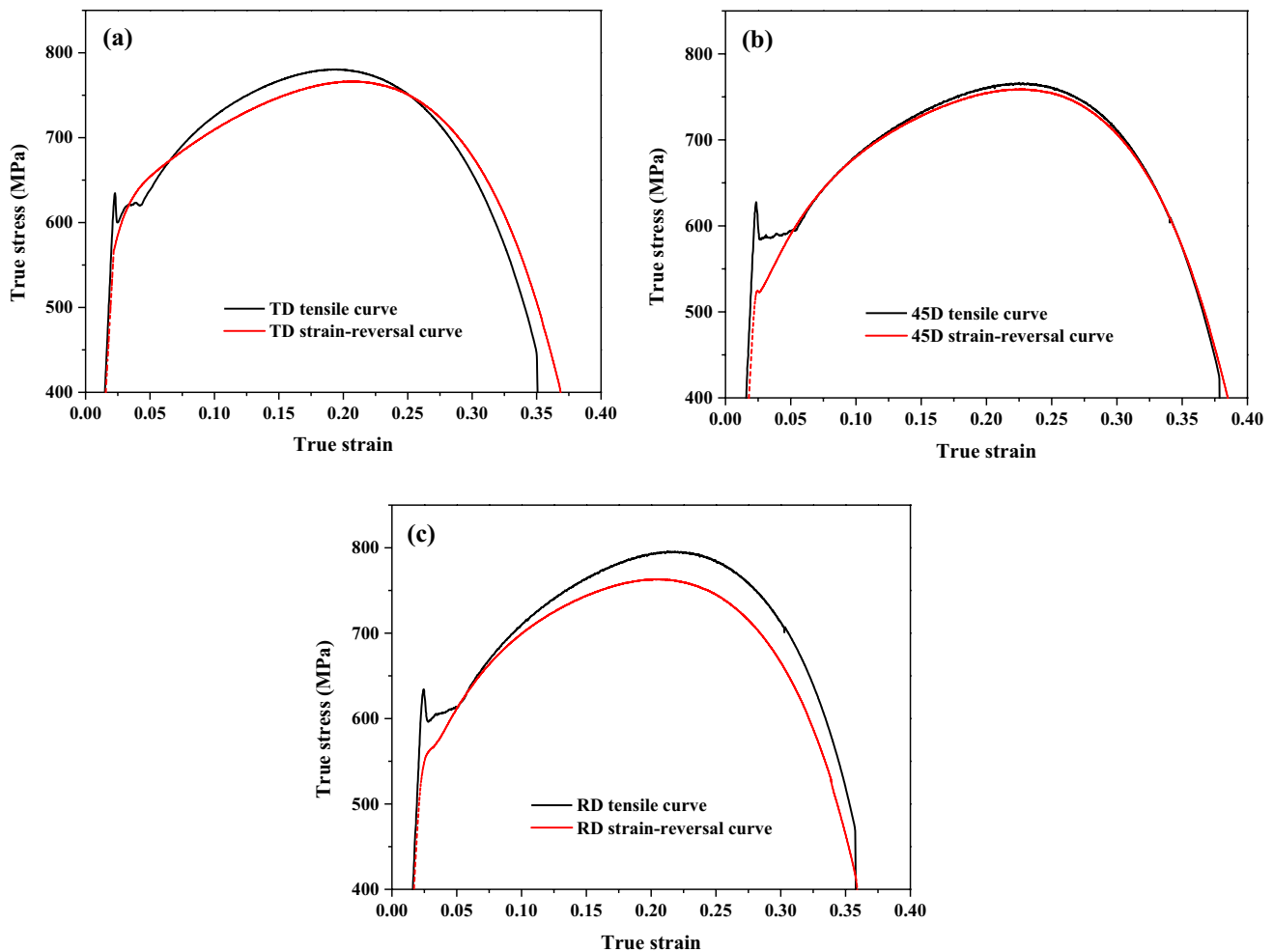


Fig. 4 Comparison of stress–strain curves obtained from tensile tests and strain-reversal tests along different loading directions: of **a** TD, **b** 45D, and **c** RD

be activated; among them, the $\{110\}$ plane has the highest atomic density, followed by the $\{112\}$ and $\{123\}$ planes [28–30]. However, the $\{100\}$ plane of a BCC structure is not a perfectly close-packed plane, unlike the $\{111\}$ plane of an FCC structure and the $\{0001\}$ plane of a hexagonal close-packed (HCP) structure. Therefore, the dominantly activated slip plane in each grain during plastic deformation of BCC metals can differ according to the strain state of that particular grain, although the active slip direction is the same in all the grains: $\langle 111 \rangle$; this is termed the $\langle 111 \rangle$ pencil glide phenomenon of BCC metals [31–33]. However, the active slip systems during $\langle 111 \rangle$ pencil glide are determined by the crystallographic orientations of individual grains and the direction of the strain imposed in the grains. Therefore, it is necessary to identify the complicated slip behaviors in BCC metals by considering the activities of the $\{112\} \langle 111 \rangle$ and $\{123\} \langle 111 \rangle$ slip systems, having relatively lower atomic densities, as well as that of the $\{110\} \langle 111 \rangle$ slip system, having the highest atomic density, because the former two

slip systems can also operate during deformation. Many previous studies have demonstrated that the results of slip behavior analysis under the assumption of $\langle 111 \rangle$ pencil glide, in which two or more slip systems are considered instead of only the $\{110\} \langle 111 \rangle$ slip system, are consistent with the experimental results for BCC metals such as interstitial-free steels or low-carbon steels [32, 34–36]. However, in the present study, the activity of $\{123\} \langle 111 \rangle$ slip system is not considered in the analysis of the deformation behavior, because it is known that the $\{123\} \langle 111 \rangle$ slip system is rarely activated at low temperatures [37].

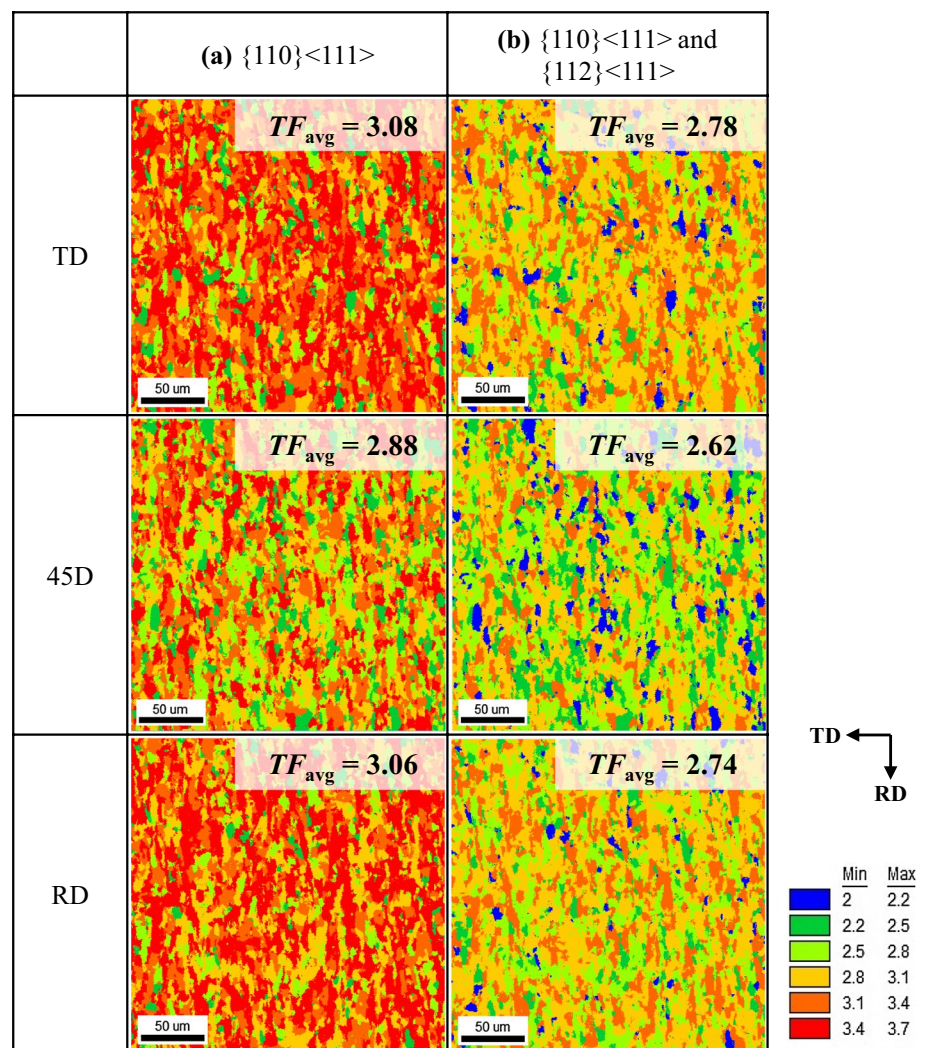
The yield and tensile behaviors of a polycrystalline material can be analyzed using the average value of Schmid factors of a number of randomly oriented single crystals [38]. However, in a polycrystalline material consisting of numerous grains, strain incompatibility between neighboring grains occurs during plastic deformation owing to the nonuniformity of lattice strains developed in individual grains [39–41]. Accordingly, in the present study, the deformation

behavior is analyzed using the Taylor factor, which satisfies the condition of strain compatibility between all the grains; the Taylor model assumes that all the individual grains of a polycrystalline material are subjected to the same strain with the activation of multiple slip systems in each grain (i.e., the model is based on an iso-strain assumption). In addition, the Taylor model is known to be reasonable for materials showing anisotropic plastic deformation because of the activation of several deformation systems, such as dislocation slip and deformation twinning [42]. The Taylor factor of a polycrystalline material is the average of the Taylor factors of the individual grains of the material, and the Taylor factor is expressed as the ratio of the macroscopic stress to the critical resolved shear stress (CRSS). Since the flow stress is related to viscoplastic deformation, plastic deformation of grains unfavorably oriented for dislocation slip is difficult [43, 44]. Namely, when a grain has a higher Taylor factor, a higher shear stress is generally required to plastically deform the grain, because the Taylor factor represents the degree of resistance to plastic deformation of a polycrystalline

material. Consequently, grains having a lower Taylor factor deform more easily than do those having a higher Taylor factor [44–46].

Figure 5 shows the Taylor factor maps obtained by EBSD analysis under deformation conditions along the TD, 45D, and RD when only the $\{110\} \langle 111 \rangle$ slip system and both the $\{110\} \langle 111 \rangle$ and the $\{112\} \langle 111 \rangle$ slip systems are activated. In all the loading directions, the average Taylor factors calculated under the condition of coactivation of the $\{110\} \langle 111 \rangle$ and $\{112\} \langle 111 \rangle$ slip systems (2.78, 2.62, and 2.74 for the TD, 45D, and RD samples, respectively) are lower than those under the condition of activation of only the $\{110\} \langle 111 \rangle$ slip system (3.08, 2.88, and 3.06 for the TD, 45D, and RD samples, respectively) (Fig. 5). This means that although the $\{110\} \langle 111 \rangle$ slip system is known to be the primary slip system in BCC metals, the activation of the $\{112\} \langle 111 \rangle$ slip system plays an important role in reducing the resistance to plastic deformation. Under both the slip conditions, i.e., under the activation only the $\{110\} \langle 111 \rangle$ slip system and under the coactivation of

Fig. 5 Taylor factor maps under deformation along TD, 45D, and RD when **a** only $\{110\} \langle 111 \rangle$ slip system is activated during plastic deformation and **b** both $\{110\} \langle 111 \rangle$ and $\{112\} \langle 111 \rangle$ slip systems are activated during plastic deformation. TF_{avg} denotes the average Taylor factor



the $\{110\} \langle 111 \rangle$ and $\{112\} \langle 111 \rangle$ slip systems, the Taylor factor of the 45D sample is lower than those of the TD and RD samples. This indicates that dislocation slips are activated on the $\{110\}$ and $\{112\}$ planes more easily when external loading is applied to the steel sheet along the 45D than when it is applied along the TD and RD. As a result, the yield strength of the 45D sample (587 MPa) is lower than those of the other samples (605 MPa and 596 MPa for the TD and RD samples, respectively) (Fig. 3 and Table 1). Furthermore, since the RD sample has a slightly lower Taylor factor than the TD sample, the yield strength of the RD sample is lower than that of the TD sample. These results demonstrate that the slip activity during deformation varies considerably with the loading direction owing to the rolling texture of the steel sheet, which consequently results in anisotropy of the yield strength of the material depending on the direction of the applied external loading.

The Taylor factor distributions under the conditions of activation of the only $\{110\} \langle 111 \rangle$ slip system and coactivation of the $\{110\} \langle 111 \rangle$ and $\{112\} \langle 111 \rangle$ slip systems are shown in Fig. 6. In all the samples, the volume fractions of grains with a high Taylor factor of 3.4 become 0 when both $\{110\} \langle 111 \rangle$ and $\{112\} \langle 111 \rangle$ are the active slip

systems. As mentioned above, the average Taylor factor of the 45D sample is lower than those of the other two samples (Fig. 5); in particular, under the condition of coactivation of the $\{110\} \langle 111 \rangle$ and $\{112\} \langle 111 \rangle$ slip systems, the volume fraction of grains with Taylor factors lower than 2.2 is 0.221 in the 45D sample, which is more than twice those in the other two samples (0.092 and 0.077 for the TD and RD samples, respectively) (Fig. 6). This means that the number of easily deformable grains is larger when the material is deformed along the 45D than when it is deformed along the TD and RD. Under the condition of coactivation of the two slip systems, though the volume fraction of grains with a Taylor factor of 3.1 is larger in the RD sample than in the TD sample, the volume fraction of grains with a Taylor factor of 2.8 is much larger in the TD sample than in the RD sample (Figs. 6a, c); as a result, the average Taylor factor of the TD sample (2.78) is slightly higher than that of the RD sample (2.74) (Fig. 5). Therefore, the order of the average Taylor factor for dislocation slip in the samples with different loading directions is consistent with that of the yield strength of the samples (i.e., TD > RD > 45D). Meanwhile, as the Lüders strain occurs during the slip activity, the Lüders strain of the 45D sample becomes larger than

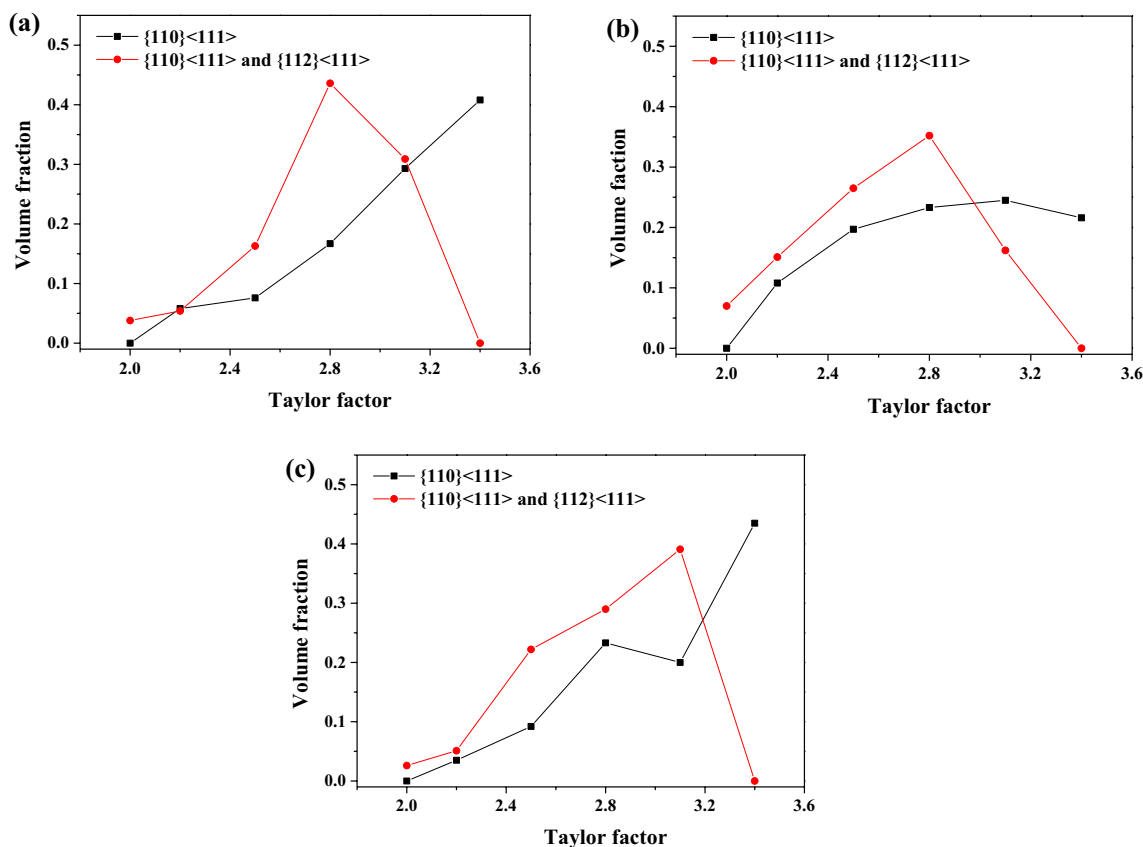


Fig. 6 Taylor factor distributions under deformation along **a** TD, **b** 45D, and **c** RD when only $\{110\} \langle 111 \rangle$ slip system is activated and when both $\{110\} \langle 111 \rangle$ and $\{112\} \langle 111 \rangle$ slip systems are activated during plastic deformation

those of the other samples because of the more vigorous slip activity in the 45D sample, which has a lower Taylor factor. The Lüders strain of the samples decreases in the following order: 45D > RD > TD; this order is consistent with the results of Taylor factor analysis of the samples. Correspondingly, the Bauschinger effect is also more pronounced in the 45D sample owing to the easy dislocation movement induced by its lower Taylor factor.

4.2 Determination of Slip Activation and Texture Evolution by VPSC Simulation

The activation of each slip system was analyzed via simulations using the VPSC model, and the simulation results were compared with the experimental results. A self-consistent polycrystalline model, which considers an interacting cluster of grains surrounded by a homogeneous matrix, was originally formulated by Molinari et al. [47] and extended by Lebensohn and Tomé [17, 18]. For interpreting the interaction between the grains and their surroundings, the VPSC model assumes that each grain is an ellipsoidal inclusion surrounded by a homogeneous effective medium (HEM) and that the formulation includes interaction equations of the linearly related stress and strain rates of the grain and the HEM. In addition, since plastic deformation in the VPSC model occurs via the physical shear mechanisms of slip and twinning, the texture evolution during deformation can be predicted through VPSC simulation. In this study, the activities of the $\{110\} \langle 111 \rangle$ and $\{112\} \langle 111 \rangle$ slip systems during deformation are identified using the VPSC model based on the VPSC code developed by Lebensohn and Tomé [17, 18]. In the simulation, the similar CRSS value is assigned to the $\{110\} \langle 111 \rangle$ and $\{112\} \langle 111 \rangle$ slip systems because the CRSS values of these two slip systems in ferrite are nearly identical, i.e., $CRSS_{\{110\}} = (1.0 \pm 0.1) \times CRSS_{\{112\}}$ [48]. On the basis of these concepts, the Voce hardening model is used to describe the deformation behavior under each strain mode in a grain; the values of the hardening parameters (i.e., τ_0 , τ_1 , θ_0 , and θ_1) and elastic stiffness used for VPSC simulations are presented in Table 2 [49–51].

Figure 7 shows the X-ray diffraction (XRD) (110) pole figure of the rolled steel sheet; this rolling texture was used as the initial texture in the VPSC simulation. The average numbers of active slip systems in a grain are obtained via

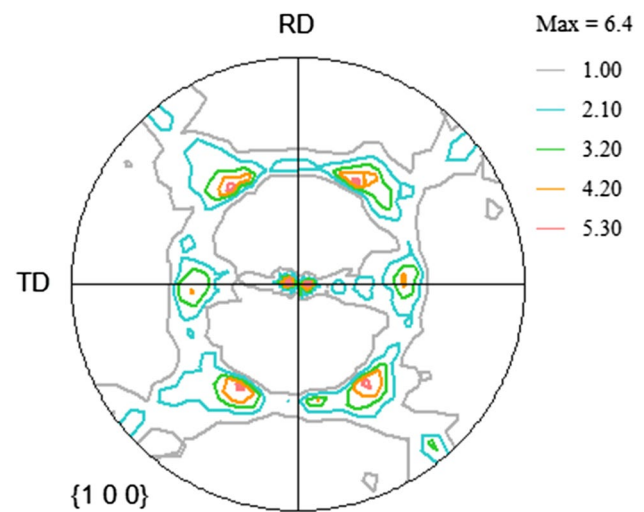


Fig. 7 XRD (110) pole figure of API X70 steel sheet, where the rolling texture was used as the initial texture for VPSC simulation

VPSC simulation by inputting the strain tensors in the tensile and compressive deformation modes along the TD, 45D, and RD (Fig. 8). In this simulation, both the $\{110\} \langle 111 \rangle$ and the $\{112\} \langle 111 \rangle$ slip systems are considered as active slip systems in order to reflect the $\langle 111 \rangle$ pencil glide during deformation. The simulation results reveal that in both the tensile and the compression deformation modes, the average number of slip systems activated in each grain during deformation is highest in the 45D sample (~ 7.4), followed by the RD sample (~ 6.6) and TD sample (~ 5.9) (Fig. 8). Accordingly, the Lüders strain produced during tensile deformation can propagate more easily in the 45D sample than in the other two samples because more dislocations can be formed by the activation of several slip variants in the 45D sample. This simulation result agrees well with the experimental result that the Lüders strain of the 45D sample is larger than those of the other two samples (Fig. 3). The relative activities of the $\{110\} \langle 111 \rangle$ and $\{112\} \langle 111 \rangle$ slip systems in the tensile and compressive deformation modes are shown in Fig. 9. The relative activity of the $\{112\} \langle 111 \rangle$ slip system during deformation is higher than 0.6 in all the loading directions and in both the tensile and the compressive deformation modes, which indicates that the $\{112\} \langle 111 \rangle$ is a dominant slip system in the steel sheet with the rolling

Table 2 Material parameters used for VPSC simulations

Slip system	T_0 (MPa)	T_1 (MPa)	θ_0	θ_1	Elastic stiffness (GPa) [49]		
					C_{11}	C_{12}	C_{44}
$\{110\} \langle 111 \rangle$	250	170	70	5.0	236.9	140.6	116.0
$\{112\} \langle 111 \rangle$	270	170	70	5.0			

T_0 , T_1 , θ_0 , and θ_1 denote the initial CRSS, back-extrapolated CRSS, initial hardening rate, and asymptotic hardening rate, respectively

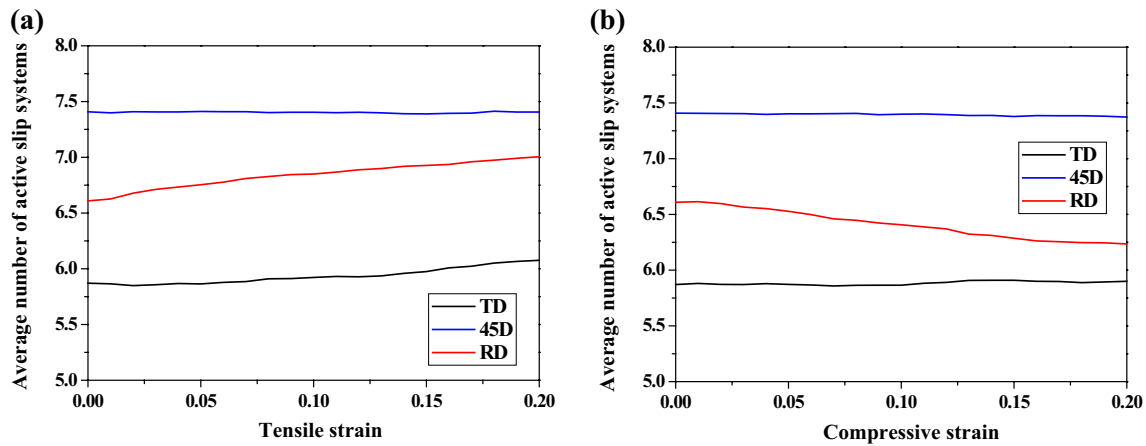


Fig. 8 Average numbers of active slip systems in **a** tensile and **b** compressive deformation modes along TD, 45D, and RD, which were estimated by VPSC simulation

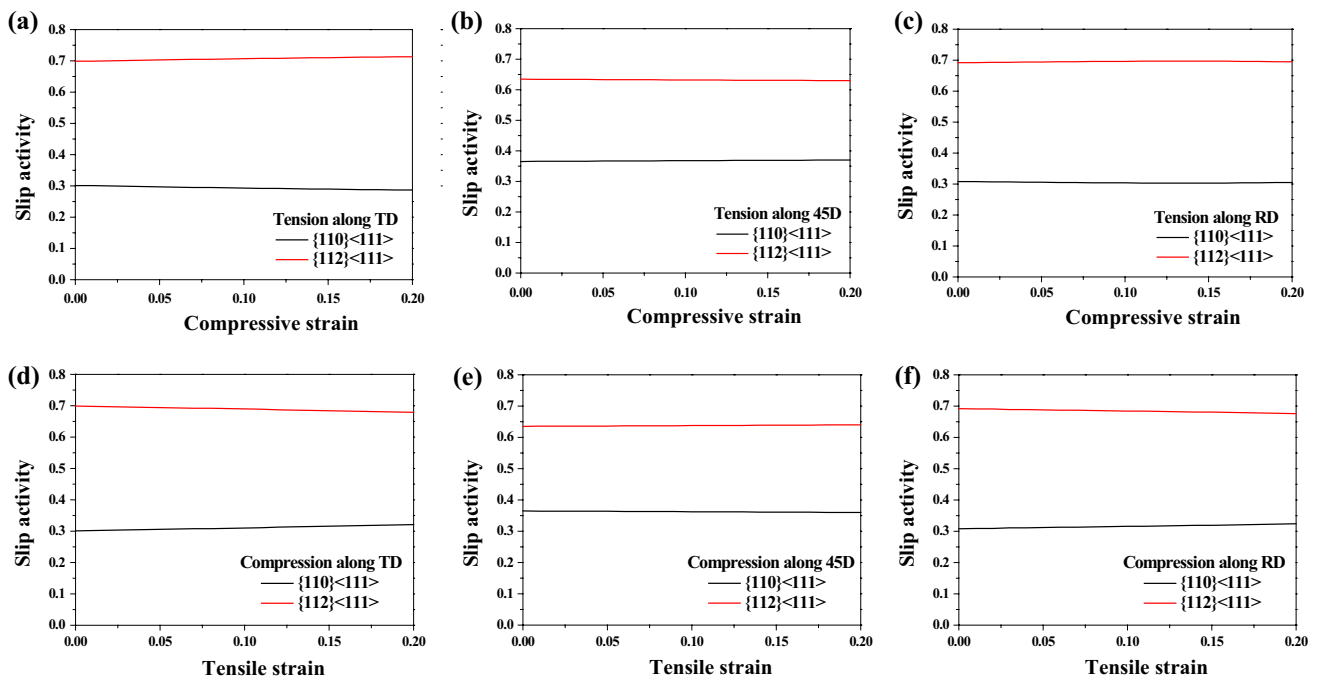


Fig. 9 Relative activities of $\{110\}\langle 111\rangle$ and $\{112\}\langle 111\rangle$ slip systems in **a–c** tensile and **d–f** compressive deformation modes along **a, d** TD, **b, e** 45D, and **c, f** RD, which were estimated by VPSC simulation

texture. This significant role of the $\{112\}\langle 111\rangle$ slip system in the deformation behavior of the steel sheet is consistent with the Taylor factor analysis results (Figs. 5 and 6). In addition, the glide of dislocations formed by precompression is easier in the 45D sample than in the other two samples, which leads to a larger reduction in the yield strength under subsequently applied reverse tensile loading. Namely, since the texture variation caused by imposition of a small amount of compressive strain (2%–3%) is negligible, the glide of the formed dislocations in the reverse direction also occurs

more easily in the 45D sample; consequently, the Bauschinger effect in the 45D sample becomes stronger than those in the RD and TD samples. This indicates that the simulation results of the number of active slip systems agree well with the experimental results of the Bauschinger effect estimated from the strain-reversal tests of the samples.

Figure 10 shows the experimentally measured and VPSC-simulated textures developed during tensile deformation. The initial texture in the simulation, which is similar to the texture before deformation in the experiment, transforms to

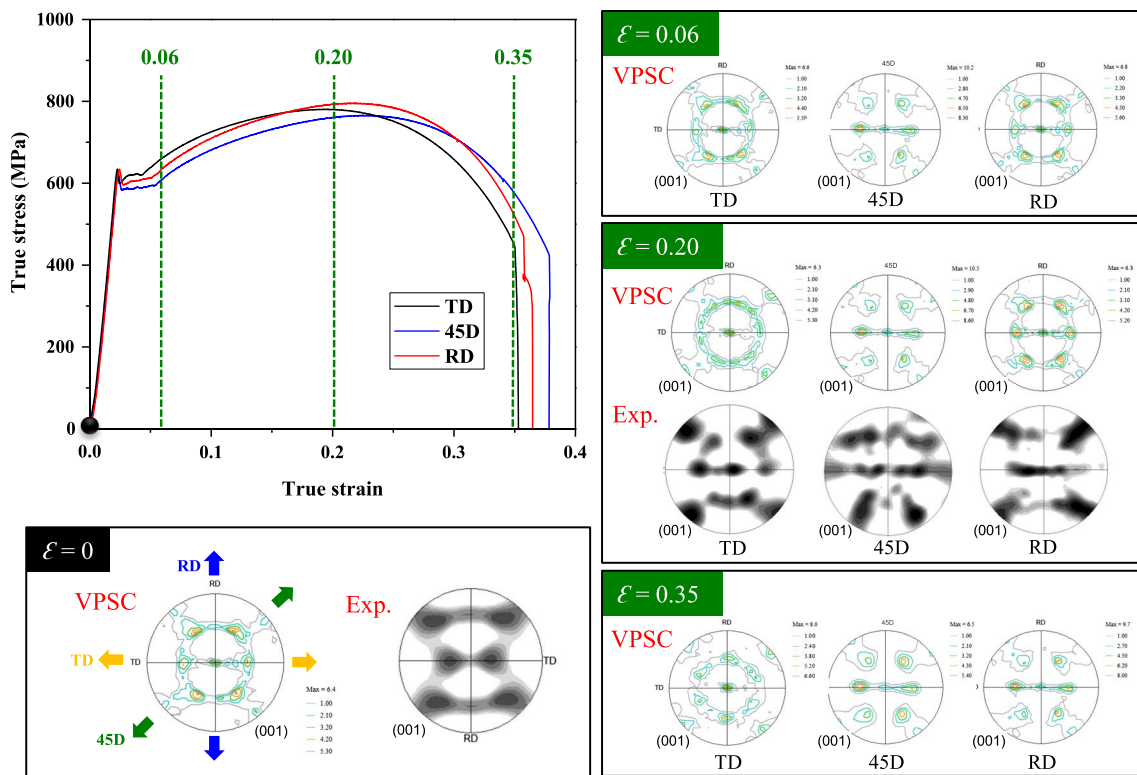


Fig. 10 VPSC simulation results of texture evolution during tensile deformation along TD, 45D, and RD. The figure shows a comparison of the simulation and experimental results of texture at a strain of 0.20

different textures depending on the applied loading direction during deformation. At a strain of 0.20, at which the stress level is close to the ultimate tensile strengths of the samples, the TD sample has high-intensity (100) poles at circumferential positions at an angle of 45° from the ND. In contrast, although the relatively large strain of 0.20 is applied to the samples, the texture of the RD sample remains nearly unchanged. In the 45D sample, strongly developed (100) poles aligned along the direction perpendicular to the 45D appear. These simulation results of texture at the strain of 0.2, which are calculated by considering the $\langle 111 \rangle$ pencil glide of the coactivated $\{110\} \langle 111 \rangle$ and $\{112\} \langle 111 \rangle$ slip systems, are consistent with the actual textures measured in the 20% tensioned samples (Fig. 10). In addition, it can be seen from the VPSC simulation results that the texture developed during tensile deformation changes considerably with the applied loading direction and the initially developed texture (at a strain of 0.06) remains almost unchanged until the fracture stage (at a strain of 0.35). The good agreement between the results of simulation performed by consideration of the $\langle 111 \rangle$ pencil glide and the experimental results indicates that the $\{112\} \langle 111 \rangle$ slip system plays an important role in the plastic deformation and texture evolution of the API steel sheet and that this $\{112\} \langle 111 \rangle$ slip system should be considered along with the $\{110\} \langle 111 \rangle$ slip

system in order to more clearly understand the plastic deformation behavior of BCC metals with a rolling texture.

5 Conclusion

This study investigates the plastic deformation behavior and Bauschinger effect along three different loading directions in a rolled API steel sheet with a rolling texture. The material exhibits discontinuous yielding behavior during tension in all the loading directions. However, the 45D sample has a lower yield strength and larger Lüders strain than the RD and TD samples, which is attributed to the lower Taylor factor for dislocation slip in the 45D sample. The decrease in the yield strength caused by the Bauschinger effect is largest in the 45D sample, followed by the RD and TD samples. This is because when plastic deformation is applied along the 45D, more slip systems can be activated under both tension and compression conditions, which facilitates the movement of the previously formed dislocations during strain-reversal tests. The variation in texture during tension is also significantly dependent on the applied loading direction. The results of Taylor factor analysis and VPSC simulation demonstrate that the $\{112\} \langle 111 \rangle$ slip system is vigorously activated during plastic deformation and that its activation

plays an important role in the deformation behavior and yield strength of the material.

Acknowledgements This work was supported by National Research Foundation of Korea (NRF) grants funded by the Korean government (MSIP, South Korea) (Nos. 2017R1A4A1015628 and 2019R1H1A1080264).

References

- N. Andou, H. Chino, C. Hamamoto, H. Majima, R. Nomura, H. Haga, N. Mizuhashi, S. Fujimori, Y. Kitamura, *Trans. Iron Steel Inst. Jpn.* **26**, 445 (1986)
- H. Akasaki, *Nippon Steel Tech. Report* **90**, 75 (2004)
- H. Brauer, H. Lobbe, *Oil and Gas Pipelines* (Wiley, Hoboken, 2015)
- D.E. Orowan, *International conference on stresses fatigue metal*, Amsterdam, 59, 1959
- A.W. Sleeswyk, M.R. James, D.H. Plantinga, W.S.T. Maathuis, *Acta Metall.* **26**, 1265 (1978)
- A. Abel, H. Muir, *Phil. Mag.* **26**, 489 (1972)
- R.E. Stoltz, R.M. Pelloux, *Metall. Mater. Trans.* **7**, 1295 (1976)
- A.A. Mamuna, R.J. Moata, J. Kelleherb, P.J. Boucharda, *Mater. Sci. Eng., A* **707**, 576 (2017)
- J.K. Mahato, P.S. De, A. Sarkar, A. Kundu, P.C. Chakraborti, *Int. J. Fatigue* **83**, 42 (2016)
- J.P. Ormandy, Thesis for the degree of master of philosophy, University of Birmingham, 2000
- K. Park, Y. Jeo, *J. Korean Inst. Met. Mater.* **36**, 1777 (1998)
- T.C. Harrison, R.T. Weiner, G.D. Fearnehough, *J. Iron. Steel Res. Int.* **210**, 334 (1972)
- C.W. Choi, H.J. Koh, S. Lee, *Metall. Mater. Trans. A* **31**, 2669 (2000)
- K. Nakajima, W. Mizutani, T. Kikuma, H. Matumoto, *Trans. Iron Steel Inst. Jpn.* **15**, 1 (1975)
- A.G. Kostryzhev, Thesis for the degree of doctor of philosophy, University of Birmingham, 2009
- A. Takekazu, N. Kimihiro, Y. Koji, S. Nobuhisa, *JFE Tech. Report* **18**, 23 (2013)
- R.A. Lebensohn, C.N. Tomé, *Acta Metall. Mater.* **41**, 2611 (1993)
- C.N. Tomé, R.A. Lebensohn, U.F. Kocks, *Acta Metall. Mater.* **39**, 2667 (1991)
- I.L. Dillamore, W.T. Roberts, *Acta Metall.* **12**, 281 (1964)
- E.O. Hall, *Yield Point Phenomena in Metals and Alloys* (Macmillan, London, 1970)
- A.H. Cottrell, B.A. Bilby, *Proc. Phys. Soc. A* **62**, 49 (1949)
- A.H. Cottrell, Report of a conference on strength of solids, Physical Society, London, 1948
- A.H. Cottrell, A.T. Churchman, *Nature* **167**, 943 (1951)
- W. Luders, J. Dinglers, *Polytech* **155**, 18 (1860)
- M.C. Mataya, M.J. Carr, *Mater. Sci. Eng.* **57**, 205 (1983)
- D. Raabe, K. Lucke, *Scr. Metall. Mater.* **26**, 1221 (1992)
- R.G. Bruna, REM: R Esc. Minas **64**(1), 57 (2011)
- A.G. Jackson, *Handbook of Crystallography* (Springer, New York, 1991)
- J.P. Hirth, J. Lothe, *Theory of Dislocations*, 2nd edn. (Wiley, New York, 1982)
- D. Hull, D.J. Bacon, *Introduction to Dislocations*, 4th edn. (Butterworth einemann, Oxford, 2001)
- P. Gilormini, B. Bacroix, J.J. Jonas, *Acta Metall.* **36**(2), 231 (1988)
- A.D. Rollett, U.F. Kocks, *Proc. Int. Conf. Texture. Mater.* **8**, 375 (1988)
- E.J. Mittemeijer, *Fundamentals of Materials Science* (Springer, Berlin, 2011)
- E.A. Calnan, C.J.B. Clew, *Phil. Mag.* **42**, 616 (1951)
- A.J. Opinsky, R. Smoluchowski, *J. App. Phys.* **22**(12), 1488 (1951)
- I.L. Dillamore, H. Katoh, *Metal Sci.* **8**, 73 (1974)
- D. Ali, M.Z. Nasreen, *J. Mater. Sci.* **46**, 3812 (2011)
- J.F. Bishop, R. Hill, *Phil. Mag.* **42**, 1298 (1951)
- T. Leffers, R.A. Lebensohn, *Proc. Int. Conf. Texture. Mater.* **11**, 307 (1996)
- G.I. Taylor, *J. Inst. Metals* **62**, 307 (1938)
- G. Winther, L. Margulies, S. Schmidt, H.F. Poulsen, *Acta Mater.* **52**(10), 2863 (2004)
- H. Wang, P.D. Wu, C.N. Tomé, Y. Huang, *J. Mech. Phys. Solids* **58**(4), 594 (2010)
- S. Biroasca, *Proc. Int. Conf. Texture. Mater.* **17**, 143 (2014)
- J. Hirsch, K. Locke, M. Hatherly, *Acta Metall.* **36**(11), 2905 (1988)
- H. Mecking, U.F. Kocks, C. Hartig, *Scr. Mater.* **35**(4), 465 (1996)
- B. Clausen, *Characterisation of Polycrystal Deformation* (RISO reports, Roskilde, 1997)
- A. Molinari, G.R. Canova, S. Ahzi, *Acta Metall.* **35**, 2983 (1987)
- C. Du, F. Maresca, M.G.D. Geers, J.P.M. Hoefnagels, *Acta Mater.* **146**, 341 (2018)
- G. Simmons, H. Wang, *Single Crystal Elastic Constants and Calculated Aggregate Properties; A Handbook* (MIT Press, Cambridge, 1971)
- G.P. Kang, K. Lee, Y.H. Kim, S.J. Park, K.S. Shin, *Met. Mater. Int.* **23**(5), 930 (2017)
- Z.H. Cong, N. Jia, X. Sun, Y. Ren, J. Almer, Y.D. Wang, *Met. Mater. Trans. A* **40**, 1383 (2009)

Publisher's Note Springer Nature remains neutral with regard to jurisdictional claims in published maps and institutional affiliations.